Pfeuffer, I., Klein-Hessling, S., Heinfling, A., Chuvpilo, S., Escher, C., Brabletz, T., Hentsch, B., Schwarzenbach, H., Matthias, P., and Serfling, E. (1994). Octamer factors exert a dual effect on the IL-2 and IL-4 promoters. *J. Immunol.* **153:**5572–5585.

Pirsch, J. D., Miller, J., Deierhoi, M. H., Vincenti, F., and Filo, R. S. (1997). A comparison of tacrolimus (FK506) and cyclosporine for immunosuppression after cadaveric renal transplantation. FK506 Kidney Transplant Study Group. *Transplantation* **63:**977–983.

Ramsauer, M., Krause, D., and Dermietzel, R. (2002). Angiogenesis of the blood-brain barrier *in vitro* and the function of cerebral pericytes. *FASEB J.* **16:**1274–1276.

Schinkel, A. H. (1999). P-Glycoprotein, a gatekeeper in the blood-brain barrier. *Adv. Drug Deliv. Rev.* **36:**179–194.

Shuto, H., Kataoka, Y., Kanaya, A., Matsunaga, K., Sueyasu, M., and Oishi, R. (1998). Enhancement of serotonergic neural activity contributes to cyclosporine-induced tremors in mice. *Eur. J. Pharmacol.* **341:**33–37.

Shuto, H., Kataoka, Y., Fujisaki, K., Nakao, T., Sueyasu, M., Miura, I., Watanabe, Y., Fujiwara, M., and Oishi, R. (1999). Inhibition of GABA system involved in cyclosporine-induced convulsions. *Life Sci.* **65:**879–887.

Smith, R. S., Jr., Agata, J., Xia, C. F., Chao, L., and Chao, J. (2005). Human endothelial nitric oxide synthase gene delivery protects against cardiac remodeling and reduces oxidative stress after myocardial infarction. *Life Sci.* **76:**2457–2471.

Tatsuta, T., Naito, M., Oh-hara, T., Sugawara, I., and Tsuruo, T. (1992). Functional involvement of P-glycoprotein in blood-brain barrier. *J. Biol. Chem.* **267:**20383–20391.

The U.S. Multicenter FK506 Liver Study Group. (1994). A comparison of tacrolimus (FK 506) and cyclosporine for immunosuppression in liver transplantation. *N. Engl. J. Med.* **331:**1110–1115.

Thomas, W. E. (1999). Brain macrophages: On the role of pericytes and perivascular cells. *Brain Res. Brain Res. Rev.* **31:**42–57.

Tsuboi, A., Muramatsu, M., Tsutsumi, A., Arai, K., and Arai, N. (1994). Calcineurin activates transcription from the GM-CSF promoter in synergy with either protein kinase C or NF-kappa B/AP-1 in T cells. *Biochem. Biophys. Res. Commun.* **199:**1064–1072.

Untergasser, G., Gander, R., Lilg, C., Lepperdinger, G., Plas, E., and Berger, P. (2005). Profiling molecular targets of TGF-b1 in prostate fibroblast-to-myofibroblast transdifferentiation. *Mech. Ageing Dev.* **126:**59–69.

Cellular and Molecular Neurobiology, Vol. 27, No. 3, May 2007 (© 2007)
DOI: 10.1007/s10571-007-9139-z

Rapid Communication

An Inhibitory Role of Nitric Oxide in the Dynamic Regulation of the Blood-Brain Barrier Function

Atsushi Yamauchi,[1] Shinya Dohgu,[1] Tsuyoshi Nishioku,[1] Hideki Shuto,[1] Mikihiko Naito,[2] Takashi Tsuruo,[2] Yasufumi Sawada,[3] and Yasufumi Kataoka[1,4]

Received June 2, 2006; accepted June 19, 2006; Published online: February 23, 2007

SUMMARY

1. The present study aimed at elucidating the effect of nitric oxide (NO) on blood-brain barrier (BBB) function with mouse brain capillary endothelial (MBEC4) cells.

2. Histamine (20–100 μM) evoked NO production (1.6–7 μM) in MBEC4 cells in a dose-dependent manner.

3. The permeability coefficient of sodium fluorescein for MBEC4 cells and the cellular accumulation of rhodamine 123 in MBEC4 cells were increased dose-dependently by the addition of NO solutions (14 and 28 μM) every 10 min during a 30-min period.

4. The present study demonstrated that NO increased the permeability and inhibited the P-glycoprotein efflux pump of brain capillary endothelial cells, suggesting that NO plays an inhibitory role in the dynamic regulation of the BBB function.

KEY WORDS: nitric oxide; blood-brain barrier (BBB); permeability; P-glycoprotein; mouse brain endothelial cells.

INTRODUCTION

The blood-brain barrier (BBB) contributes to brain homeostasis and fulfills a protective function by regulating the access of solutes and toxic substances to the central nervous system. The BBB is formed by brain capillary endothelial cells, which are closely sealed by tight junctions (Pardridge, 1999). The tight junctions in the

[1] Department of Pharmaceutical Care and Health Sciences, Faculty of Pharmaceutical Sciences, Fukuoka University, 8-19-1 Nanakuma, Jonan-ku, Fukuoka 814-0180, Japan.
[2] Institute of Molecular and Cellular Biosciences, University of Tokyo, Bunkyo-ku, Tokyo 113-0032, Japan.
[3] Laboratory of Drug Imformatics, Graduate School of Pharmaceutical Sciences, The University of Tokyo, 3-14-15 Hongo, Bunkyo-ku, Tokyo 113-0033, Japan.
[4] To whom correspondence should be addressed at Department of Pharmaceutical Care and Health Sciences, Faculty of Pharmaceutical Sciences, Fukuoka University, 8-19-1 Nanakuma, Jonan-ku, Fukuoka 814-0180, Japan; e-mail: ykataoka@fukuoka-u.ac.jp.

BBB prevent significant passive movement of small hydrophilic molecules from the blood to the brain, but specialized transport systems mediate the entry of essential substances such as glucose, amino acids, choline, monocarboxylic acids, amines, thyroid hormones, purine bases, and nucleosides (Tsuji and Tamai, 1999; Kusuhara and Sugiyama, 2001). The efflux transporter, P-glycoprotein (P-gp) is a key element of the molecular machinery that confers special permeability properties on the BBB. P-gp, which was initially recognized for its ability to excrete anticancer drugs from multidrug-resistant cancer cells, is strongly expressed in brain capillaries. Its expression in the BBB limits the accumulation of many hydrophobic molecules and potentially toxic substances in the brain.

Nitric oxide (NO) is a transient product of inflammatory processes, generated from L-arginine by the enzyme NO synthase (NOS). NO appears to be involved in numerous vital cellular functions including neurotransmission, blood-pressure control, and the regulation of vascular tone. The basal production of NO appears to be required for biological regulation, and yet an excess of this same molecule can be cytotoxic to organism. But the molecular mechanisms mediating NO-induced tissue injury and breakdown of the BBB are not completely understood.

In the present study, to clarify the role of NO in the dynamic regulation of the BBB, we examined effect of NO on the function of tight junctions and P-gp in mouse brain capillary endothelial (MBEC4) cells. MBEC4 cells show the highly specialized characteristics of brain microvascular endothelial cells including P-gp expression (Tatsuta *et al.*, 1992, 1994).

MATERIALS AND METHODS

A saturated NO solution (typically containing approximately 1.4 mM NO) was prepared according to Ikesue *et al.* (2000). Deionized water (2 mL) was bubbled with argon for 20 min to remove oxygen. Then, the solution was bubbled with pure NO gas for 20 min and kept in a glass flask with a rubber septum under a NO atmosphere prior to use.

MBEC4 cells, which were isolated from BALB/c mouse brain cortices and immortalized by SV40-transformation (Tatsuta *et al.*, 1992), were cultured in Dulbecco's modified Eagle's medium (DMEM; GIBCO BRL, Life Technologies, Grand Island, NY) supplemented with 10% fetal bovine serum, 100 units/mL of penicillin, and 100 μg/mL of streptomycin. They were grown in 2.5-cm^2 dish, 12-well Transwells (Costar, MA) and 24-well plates in a humidified atmosphere of 5% CO_2/95% air at 37°C.

Direct and continuous electrochemical measurement of NO was performed with a three-electrode potentiostatic EMS-100 system (BIO-LOGIC, Grenoble, France), as previously described (Ikesue *et al.*, 2000; Trevin *et al.*, 1998). In brief, confluent MBEC4 cells in a 2.5-cm^2 dish were washed three times with Krebs–Ringer solution (143.0 mM NaCl, 4.7 mM KCl, 2.5 mM $CaCl_2$, 1.0 mM NaH_2PO_4, and 11.0 mM D-glucose, pH 7.4). The dish was placed on the stage of an inverted microscope (ECLIPSE TE300, Nikon, Tokyo, Japan) mounted with an NO monitoring system. The NO-biosensor (ASTEC, Fukuoka, Japan) was positioned about 10 μm

above the cell surface. Ten minutes after treatment with 1-mM L-arginine (Sigma, St. Louis, MO), histamine (Wako, Osaka, Japan) in a volume of 10 μL was added to the cells in 1 mL of Krebs–Ringer solution with a transient mixing step to give the final concentration indicated. The level of production of NO in MBEC4 cells was monitored for a 15-min period after the addition of histamine.

MBEC4 cells (42,000 cells/cm^2) were cultured on the collagen-coated polycarbonate membrane of the Transwell insert (3.0-μm pore size, 12-well type). After 3 days, they were washed three times with serum-free medium. Cells were exposed to 5 or 10 μL of NO solution (final concentration, 14 and 28 μM, respectively) injected into the inside of the insert (luminal side) every 10 min during a 30-min period. To initiate the transport experiments, the medium was removed, and cells were washed three times with Krebs–Ringer buffer (118 mM NaCl, 4.7 mM KCl, 1.3 mM $CaCl_2$, 1.2 mM $MgCl_2$, 1.0 mM NaH_2PO_4, 25 mM $NaHCO_3$, and 11 mM D-glucose, pH 7.4). Krebs–Ringer buffer (1.5 mL) was added to the outside of the insert (abluminal side). Krebs–Ringer buffer (0.5 mL) containing 100 μg/mL of sodium fluorescein (Na-F; Sigma) was loaded on the luminal side of the insert. Samples (0.5 mL) were removed from the abluminal chamber at 10, 20, 30, and 60 min and were immediately replaced with fresh Krebs–Ringer buffer. Aliquots (5 μL) from the abluminal chamber samples were mixed with 200 μL of Krebs–Ringer buffer, and then the concentration of Na-F was determined using a multiwell fluorometer ($E_x(\lambda)$ 485 nm; $E_m(\lambda)$ 530 nm; CytoFluor Series 4000, PerSeptive Biosystems, Framingham, MA). The permeability coefficient and clearance were calculated according to the method described by Dehouck *et al.* (1992). Clearance was expressed as microliters of tracer diffusing from the luminal to abluminal chamber and was calculated from the initial concentration of tracer in the luminal chamber and final concentration in the abluminal chamber: Clearance (μL) = $[C]_A \times V_A/[C]_L$ where $[C]_L$ is the initial luminal tracer concentration, $[C]_A$ is the abluminal tracer concentration, and V_A is the volume of the abluminal chamber. During a 60-min period of the experiment, the clearance volume increased linearly with time. The average volume cleared was plotted versus time, and the slope was estimated by linear regression analysis. The slope of clearance curves for the MBEC4 monolayer was denoted by PS_{app}, where PS is the permeability-surface area product (in microliters per minute). The slope of the clearance curve with a control membrane was denoted by $PS_{membrane}$. The real PS value for the MBEC4 monolayer (PS_{trans}) was calculated from $1/PS_{app} = 1/PS_{membrane} + 1/PS_{trans}$. The PS_{trans} values were divided by the surface area of the Transwell inserts to generate the permeability coefficient (P_{trans}, in centimeters per minute).

The functional activity of P-gp was determined by measuring the cellular accumulation of rhodamine 123 (Sigma) according to the method of Fontaine *et al.* (1996). MBEC4 cells (21,000 cells/cm^2) were cultured on collagen-coated 24-well plates. Three days after seeding, they were washed three times with serum-free medium and then exposed to 14–28 μM of NO solution every 10 min during a 30-min period. The medium was removed, and the cells were washed three times with assay buffer (143 mM NaCl, 4.7 mM KCl, 1.3 mM $CaCl_2$, 1.2 mM $MgCl_2$, 1.0 mM NaH_2PO_4, 10 mM HEPES, and 11 mM D-glucose, pH 7.4). The cells were incubated with 0.5 mL of assay buffer containing 5 μM of rhodamine 123 for 60 min. Then,

the solution was removed, and the cells were washed three times with ice-cold phosphate-buffered saline and solubilized in 1 M NaOH (0.2 mL). The solution was neutralized with 1 M HCl (0.2 mL), and the rhodamine 123 content was determined using a multiwell fluorometer ($E_x(\lambda)$ 485 nm; $E_m(\lambda)$ 530 nm). The cellular protein was measured by the method of Bradford (Bradford, 1976).

The effect of the NO solution on cell viability was assessed using a WST-8 assay (Cell Counting Kit, DOJINDO, Kumamoto, Japan). A highly water-soluble formazan dye, reduced by mitochondrial dehydrogenase, was measured by determining the absorbance of each sample with a 450-nm test wavelength and a 700-nm reference wavelength.

The values are expressed as means ± SEM. Statistical analysis was performed using Student's *t*-test. One-way analysis of variance (ANOVA) followed by the Dunnett test was applied to multiple comparisons. The differences between means were considered to be significant when *P* values were less than 0.05.

RESULTS

Figure 1A shows a representative current-time curve obtained with the NO biosensor in MBEC4 cells. When L-arginine (1 mM) was added to cells 10 min before the addition of histamine, the signal became stable within 1–2 min. The NO-biosensor signal increased rapidly to reach a peak within 1 min after the injection of histamine. Following this period, the signal decreased slowly to the baseline about 5–7 min post-injection. Histamine at concentrations of 20–100 μM dose-dependently increased NO production (1.55 ± 0.65–6.94 ± 1.43 μM) in MBEC4 cells (Fig. 1B).

To evaluate effect of NO on the BBB function, the concentration and the exposure time of NO were determined on the basis of NO production evoked by histamine. When the NO solution at the final concentrations of 14 and 28 μM was added every 10 min during a 30-min period, the permeability coefficients of Na-F for MBEC4 cells increased dose-dependently to 113.6 ± 12.9 and 123.7 ± 2.8%, respectively (Fig. 2A). The exposure to NO solution had no effect on cell viability assessed with the WST-8 assay (14 μM: 93.7 ± 3.3%, 28 μM: 101.3 ± 3.2% of control).

As shown in Fig. 2B, the accumulation of rhodamine 123 in MBEC4 cells increased dose-dependently to 108.3 ± 4.8 and 164.5 ± 14.6% of the control value after a 30-min exposure to the NO solution at concentrations of 14 and 28 μM, respectively.

DISCUSSION

As shown in Fig. 1, direct and continuous electrochemical monitoring revealed that histamine stimulated MBEC4 cells to release NO over a short period (about 5 min). This phenomenon appears to be due to an activation of the constitutive endothelial form of NO synthase (eNOS) through a Ca^{2+}/calmodulin-dependent pathway in response to H_1 receptor-mediated increases in intracellular Ca^{2+} (Daum

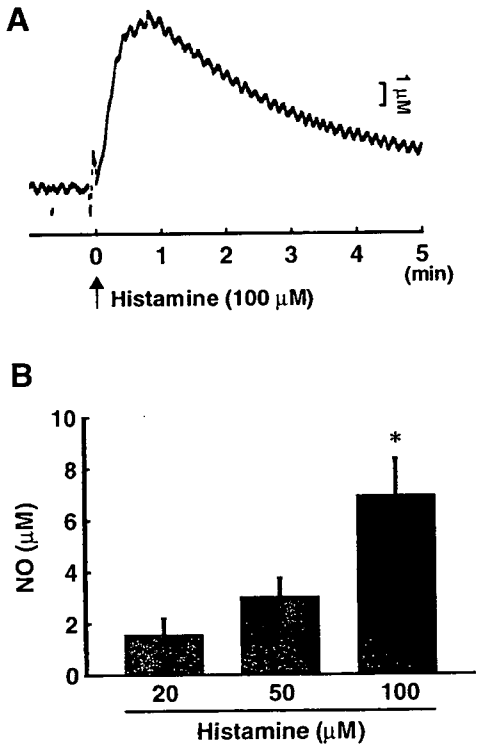

Fig. 1. Histamine-induced NO production in MBEC cells. (A) A representative differential pulse amperogram obtained using a NO biosensor shows the level of NO production evoked by histamine (100 μM). (B) Concentration-response relationship of histamine-induced NO production using direct electrochemical monitoring in MBEC cells. Values are means ± SEM (n = 3). *$p < 0.05$, significant difference from 20 μM histamine.

et al., 1983; Kishi *et al.*, 1996). Various endogenous substances including histamine stimulate NO production in the microvascular endothelium and/or glial and neuronal cells in the brain (Mayhan, 1996), probably contributing to dynamic regulation of the BBB function.

The permeability of MBEC4 cells to Na-F was apparently increased by a brief exposure to NO solutions at 2- to 4-fold the concentrations induced by histamine (Fig. 2A). The NO solutions employed here are more prominent than convenient NO donors such as sodium nitroprusside with respect to biological properties including distribution and degradation. The cell viability was not influenced by NO at the concentrations employed here (14–28 μM), suggesting that the increased paracellular permeability of MBEC4 cells was not due to the cytotoxicity of NO. Therefore, NO is highly likely to lower the functions of the tight junctions at the BBB,

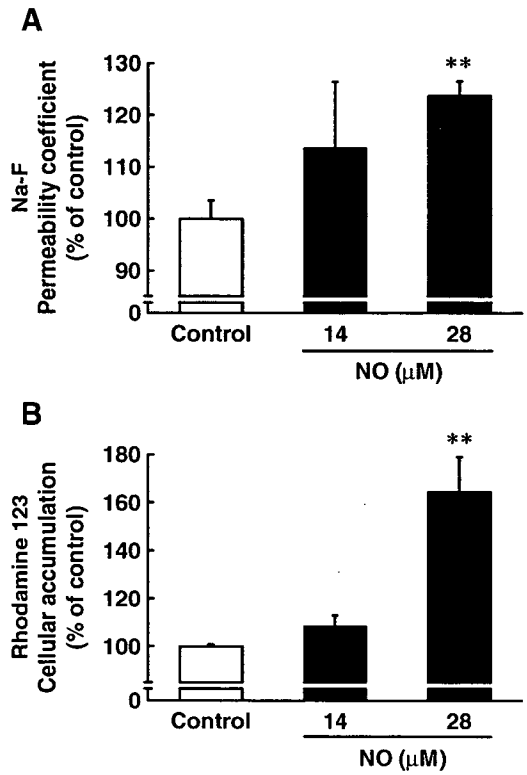

Fig. 2. Changes in the permeability coefficient of Na-F (A) and the cellular accmulation of rhodamine 123 (B) in MBEC4 cell monolayers after addition of NO solutions every 10 min during a 30-min period. Data are expressed as a percentage of the corresponding control value (A: 1.47 ± 0.21 × 10^{-4} cm/min, B: 0.95 ± 0.07 nmol/mg protein). Values are shown as means ± SEM (n = 3–18). $^{**}P < 0.01$, significant difference from control.

supporting early reports (Hurst and Fritz, 1996; Mayhan, 2000; Shukula *et al.*, 1996). The mechanisms by which NO donors increased vascular endothelial permeability involved an increase in the level of cyclic guanosine monophosphate (cGMP) (Gimeno *et al.*, 1998) or the formation of peroxynitrite (Menconi *et al.*, 1998). These substances conceivably influence the intrinsic tight junction proteins and the associated actin cytoskeleton through a direct or second signaling pathway. Further studies are required to clarify this mechanism.

In the present study, the most important finding was that the accumulation of rhodamine 123, a substrate of P-gp (Fontaine *et al.*, 1996), in MBEC4 cells was increased by treatment with NO solutions (Fig. 2B). P-gp is an energy-dependent efflux pump mediating the transportation of substances from the basement membrane to the luminal surface. NO induced a depletion of endothelial ATP by

inhibiting glyceraldehyde-3-phosphate dehydrogenase (glycolytic enzyme) activity (Hurst *et al.*, 2001). This inhibition of energy metabolism is probably associated with the NO-triggered inhibition of P-gp function.

In the present study, NO induced hyperpermeability in MBEC4 cells and inhibition of the P-gp efflux pump. These findings suggest that NO in the brain plays an inhibitory role in the dynamic regulation of the BBB function.

ACKNOWLEDGMENTS

This work was supported in part by Grants-in-Aid for Scientific Research ((B)(2) 14370789) and ((C)(2) 15590475) from JSPS, Japan, by a Grant-in-Aid for Exploratory Research (16659138) from MEXT, Japan, and by funds (No.: 031001) from the Central Research Institute of Fukuoka University.

REFERENCES

Bradford, M. M. (1976). A rapid and sensitive method for the quantitation of microgram quantities of protein utilizing the principle of protein-dye binding. *Anal. Biochem.* **72:**248–254.

Daum, P. R., Downes, C. P., and Young, J. M. (1983). Histamine-induced inositol phosholipid breakdown mirrors H1-receptor density in brain. *Eur. J. Pharmacol.* **87:**497–498.

Dehouck, M.-P., Jolliet-Riant, P., Brée, F., Fruchart J.-C., Cecchelli, R., and Tillement, J.-P. (1992). Drug transfer across the blood-brain barrier: Correlation between in vitro and in vivo models. *J. Neurochem.* **58:**1790–1797.

Fontaine, M., Elmquist, W. F., and Miller, D. W. (1996). Use of rhodamine 123 to examine the functional activity of P-glycoprotein in primary cultured brain microvessel endothelial cell monolayers. *Life Sci.* **59:**1521–1531.

Gimeno, G., Carpentier, P. H., Desquand-Billiald, S., Hanf, R., and Finet, M. (1998). L-arginine and NG-nitro-L-arginine methyl ester cause macromolecular extravasation in the microcirculation of awake hamsters. *Eur. J. Pharmacol.* **346:**275–282.

Hurst, R. D., and Fritz, I. B. (1996). Properties of an immortalized vascular endothelial/glioma cell coculture model of blood-brain barrier. *J. Cell. Physiol.* **167:**81–88.

Hurst, R. D., Azam, S., Hurst, A., and Clark, J. B. (2001). Nitric-oxide-induced inhibition of glyceraldehyde-3-phosphate dehydrogenase may mediate reduced endothelial cell monolayer integrity in an in vitro model blood-brain barrier. *Brain Res.* **894:**181–188.

Ikesue, H., Kataoka, Y., Kawachi, R., Dohgu, S., Shuto, H., and Oishi, R. (2000). Cyclosporine enhances α_1-adrenoceptor-mediated nitric oxide production in C6 glioma cells. *Eur. J. Pharmacol.* **407:**221–226.

Kishi, F., Nakaya, Y., Takahashi, A., Miyoshi, H., Nomura, M., and Saito, K. (1996). Intracellular and extracellular Ca^{2+} regulate histamine-induced release of nitric oxide in vascular endothelial cells as shown with sensitive and selective nitric oxide electrodes. *Pharmacol. Res.* **33:**123–126.

Kusuhara, H., and Sugiyama, Y. (2001). Efflux transport systems for drugs at the blood-brain barrier and blood-cerebrospinal fluid barrier (Part 1). *Drug. Discov. Today* **6:**150–156.

Mayhan, W. G. (1996). Role of nitric oxide in histamine-induced increases in permeability of the blood-brain barrier. *Brain Res.* **743:**70–76.

Mayhan, W. G. (2000). Nitric oxide donor-induced increase in permeability of the blood-brain barrier. *Brain Res.* **866:**101–108.

Menconi, M. J., Unno, N., Smith, M., Aguirre, D. E., and Fink, M. P. (1998). Nitric oxide donor-induced hyperpermeability of cultured intestinal epithelial monolayers: Role of superoxide radical, hydroxyl radical, and peroxynitrite. *Biochim. Biophys. Acta* **1425:**189–203.

Pardridge, W. M. (1999). Blood-brain barrier biology and methodology. *J. Neurovirol.* **5:**556–569.

Shukula, A., Dikshit, M., and Srimal, R. C. (1996). Nitric oxide-dependent blood-brain barrier permeability alteration in the rat brain. *Experientia* **52:**136–140.

Tatsuta, T., Naito, M., Oh-hara, T., Sugawara, I., and Tsuruo, T. (1992). Functional involvement of P-glycoprotein in blood-brain barrier. *J. Biol. Chem.* **267**:20383–20391.

Tatsuta, T., Naito, M., Mikami, K., and Tsuruo, T. (1994). Enhanced expression by the brain matrix of P-glycoprotein in brain capillary endothelial cells. *Cell Growth Differ.* **5**:1145–1152.

Trevin, S., Kataoka, Y., Kawachi, R., Shuto, H., Kumakura, K., and Oishi, R. (1998). Direct and continuous electrochemical measurement of noradrenaline-induced nitric oxide production in C6 glioma cells. *Cell. Mol. Neurobiol.* **18**:453–458.

Tsuji, A., and Tamai, I. (1999). Carrier-mediated or specialized transport of drugs across the blood-brain barrier. *Adv. Drug. Deliv. Rev.* **36**:277–290.

J Pharmacol Sci 103, 323 – 327 (2007)

Journal of Pharmacological Sciences

Short Communication

Protective Action of Indapamide, a Thiazide-Like Diuretic, on Ischemia-Induced Injury and Barrier Dysfunction in Mouse Brain Microvascular Endothelial Cells

Tsuyoshi Nishioku[1], Fuyuko Takata[1], Atsushi Yamauchi[1], Noriko Sumi[1], Ikumi Yamamoto[1], Akiko Fujino[1], Mikihiko Naito[2], Takashi Tsuruo[2,3], Hideki Shuto[1], and Yasufumi Kataoka[1,*]

[1]*Department of Pharmaceutical Care and Health Sciences, Faculty of Pharmaceutical Sciences, Fukuoka University, 8-19-1 Nanakuma, Jonan-ku, Fukuoka 814-0180, Japan*
[2]*Institute of Molecular and Cellular Biosciences, University of Tokyo, Bunkyo-ku, Tokyo 113-0032, Japan*
[3]*Cancer Chemotherapy Center, Japanese Foundation for Cancer Research, 3-10-6, Ariake, Koto-ku, Tokyo 135-8550, Japan*

Received November 20, 2006; Accepted December 28, 2006

Abstract. The aim of the present study was to elucidate the effects of indapamide on ischemic damage to the blood-brain barrier (BBB) in vitro. The ischemia/reperfusion conditions employed here significantly decreased the viability of mouse brain capillary endothelial (MBEC4) cells, an effect ameliorated by indapamide. Ischemia increased the permeability of MBEC4 cells to two cellular transport markers, sodium fluorescein and Evan's blue-albumin. Indapamide reduced the ischemia-induced hyperpermeability of cells. These results suggest that indapamide may have a protective role against ischemia-induced injury and dysfunction of the BBB.

Keywords: indapamide, ischemia, blood-brain barrier

The blood-brain barrier (BBB) greatly restricts the transport of substances between the blood and the central nervous system. The BBB is primarily formed by brain capillary endothelial cells, which are sealed closely with tight junctions (1). Disruption of the BBB can lead to edema and central nervous system pathology in conditions such as stroke. In vitro, hypoxia has been shown to increase the permeability of brain microvascular endothelial cells (2, 3). Targeting the BBB may enhance our understanding of the mechanisms that mediate ischemic brain damage and might aid the development of future treatments for stroke (4, 5).

Indapamide is an indoline derivative of chlorosulfonamide that has both diuretic and antihypertensive properties. Indapamide protects against myocardial ischemia due to its antioxidant action (6). A randomized controlled clinical trial showed that in combination, therapy with perindopril, an angiotensin-converting-enzyme inhibitor, and indapamide reduced the risk of stroke in hypertensive and non-hypertensive patients to a greater degree, compared to single drug therapy with perindopril alone (7). This clinical evidence suggests a possible involvement of indapamide in protecting against recurrent cerebrovascular disease. The present study was, therefore, aimed at evaluating the effect of indapamide on ischemia/reperfusion-induced damage to cerebral microvascular endothelial cells in vitro.

The mouse brain capillary endothelial cells used in the current study (MBEC4) show highly specialized characteristics of brain microvascular endothelial cells (8). MBEC4 cells were isolated from BALB/c mouse brain cortices and immortalized by SV40-transformation (8). Cells were cultured in Dulbecco's modified Eagle's medium (DMEM) (Invitrogen, Carlsbad, CA, USA) supplemented with 10% fetal bovine serum, 100 units /mL of penicillin, and 100 μg/mL of streptomycin. Cells were grown in collagen-coated 24-well plates (21,000 cells/cm^2, 1.8 cm^2/well; Corning, Acton, MA, USA) in a humidified atmosphere of 5% CO_2 / 95% air at 37°C. Ischemia was initiated in vitro by incubating cells with D-glucose-free Krebs-Ringer buffer (143 mM NaCl, 4.7 mM KCl, 1.3 mM $CaCl_2$, 1.2 mM $MgCl_2$, 1.0 mM

*Corresponding author. ykataoka@fukuoka-u.ac.jp
Published online in J-STAGE: March 2, 2007
doi: 10.1254/jphs.SC0060222

NaH_2PO_4, 25 mM $NaHCO_3$, and 11 mM sucrose, pH 7.4) in an anoxic incubator replaced with 5% CO_2 / 95% N_2 for 10 h at 37°C (ischemia conditions). Subsequently, cells were incubated with serum-free DMEM in 5% CO_2 / 95% air at 37°C for 1 h (reperfusion conditions). As a control, cells were incubated with normal Krebs-Ringer buffer (143 mM NaCl, 4.7 mM KCl, 1.3 mM $CaCl_2$, 1.2 mM $MgCl_2$, 1.0 mM NaH_2PO_4, 25 mM $NaHCO_3$, and 11 mM D-glucose, pH 7.4) for 10 h and subsequently incubated with serum-free DMEM for 1 h in 5% CO_2 / 95% air at 37°C (normal conditions). To test whether indapamide protects against ischemia/reperfusion-induced cell death, cells were exposed to 10 – 50 μM of indapamide (Kyoto Pharmaceutical Industries, Kyoto) or vehicle (0.25% dimethyl Sulfoxide) during conditions of ischemia and reperfusion or normal conditions. Cell viability was measured by the WST-1 assay (Cell Counting Kit-8; Dojindo, Kumamoto).

Endothelial barrier function was evaluated by measuring permeability of cells to sodium fluorescein (Na-F) and Evan's blue-albumin (EBA) as previously described (9). MBEC4 cells were grown on the collagen-coated membrane (1.1 cm^2, 0.4-μm pore size) of a Transwells™ insert (42,000 cells/cm^2, Corning) and subsequently exposed to the above-mentioned ischemia conditions for 7 h. As a control, MBEC4 cells were incubated with normal Krebs-Ringer buffer for 7 h (normal conditions). Cells were exposed to 10 – 100 μM of indapamide or vehicle during ischemia conditions or normal conditions. To initiate transport experiments, the medium was removed and cells were washed with normal Krebs-Ringer buffer. Krebs-Ringer buffer containing 100 μg /mL of Na-F (MW 376; Sigma, St. Louis, MO, USA) and 670 μg/mL EBA bound to 0.1% BSA (MW = 67 kDa) were loaded on to the luminal side of the insert. Samples were removed from the abluminal chamber at 30, 60, 90, and 120 min and immediately replaced with Krebs-Ringer buffer. The concentrations of Na-F and EBA were determined with a CytoFluor Series 4000 fluorescence multiwell plate reader [Ex(λ) 485 ± 10 nm and Em(λ) 530 ± 12.5 nm; PerSeptive Biosystems, Framingham, MA, USA] and an Opsys MR microplate reader (630 nm; DYNEX Technologies, Chantilly, VA, USA), respectively. The permeability coefficient and clearance were calculated according to the method of Dehouck et al. (10), as previously described (9).

Data are expressed as the mean ± S.E.M. Statistical analysis was performed using one-way analyses of variance (ANOVA) followed by Tukey-Kramer's post-hoc test. The difference in means was considered to be significant when the P value was less than 0.05.

As shown in Fig. 1, the ischemia (10 h)/reperfusion

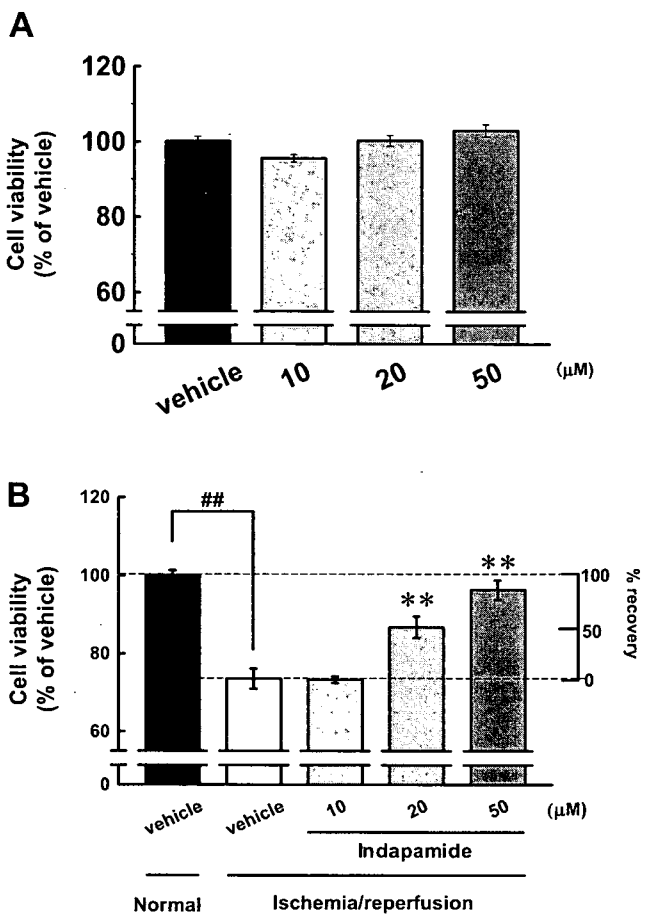

Fig. 1. Effects of indapamide on the viability of MBEC4 cells subjected to normal (A) or ischemia/reperfusion (B) conditions. Results are expressed as % of cell viability under normal conditions with vehicle treatment (% of vehicle). The % recovery is shown on the right-side of panel B and was calculated using the following equation: [% of vehicle under ischemia/reperfusion conditions with indapamide treatment – % of vehicle under ischemia/reperfusion conditions with vehicle treatment] / [% of vehicle under normal conditions with vehicle treatment – % of vehicle under ischemia /reperfusion conditions with vehicle treatment] × 100. Data are expressed as the mean ± S.E.M. (n = 8 – 20). $^{\#\#}P<0.01$, significant difference from vehicle under normal conditions. $^{**}P<0.01$, significant difference from the vehicle under ischemia/reperfusion conditions.

(1 h) conditions significantly decreased the viability of MBEC4 cells grown on collagen-coated wells, by 26.5% of cells subjected to normal conditions. The effect of indapamide on ischemia/reperfusion-induced damage in MBEC4 cells was concentration-dependent: 20 – 50 μM indapamide improved recovery by 50% – 86%. These concentrations have no effect on cell viability under normal conditions. As shown in Fig. 2, a 7-h period of ischemia resulted in increased permeability of MBEC4 cells grown on collagen-coated membranes to Na-F (paracellular transport marker) and EBA (transendothelial transport marker). Following ischemia, the perme-

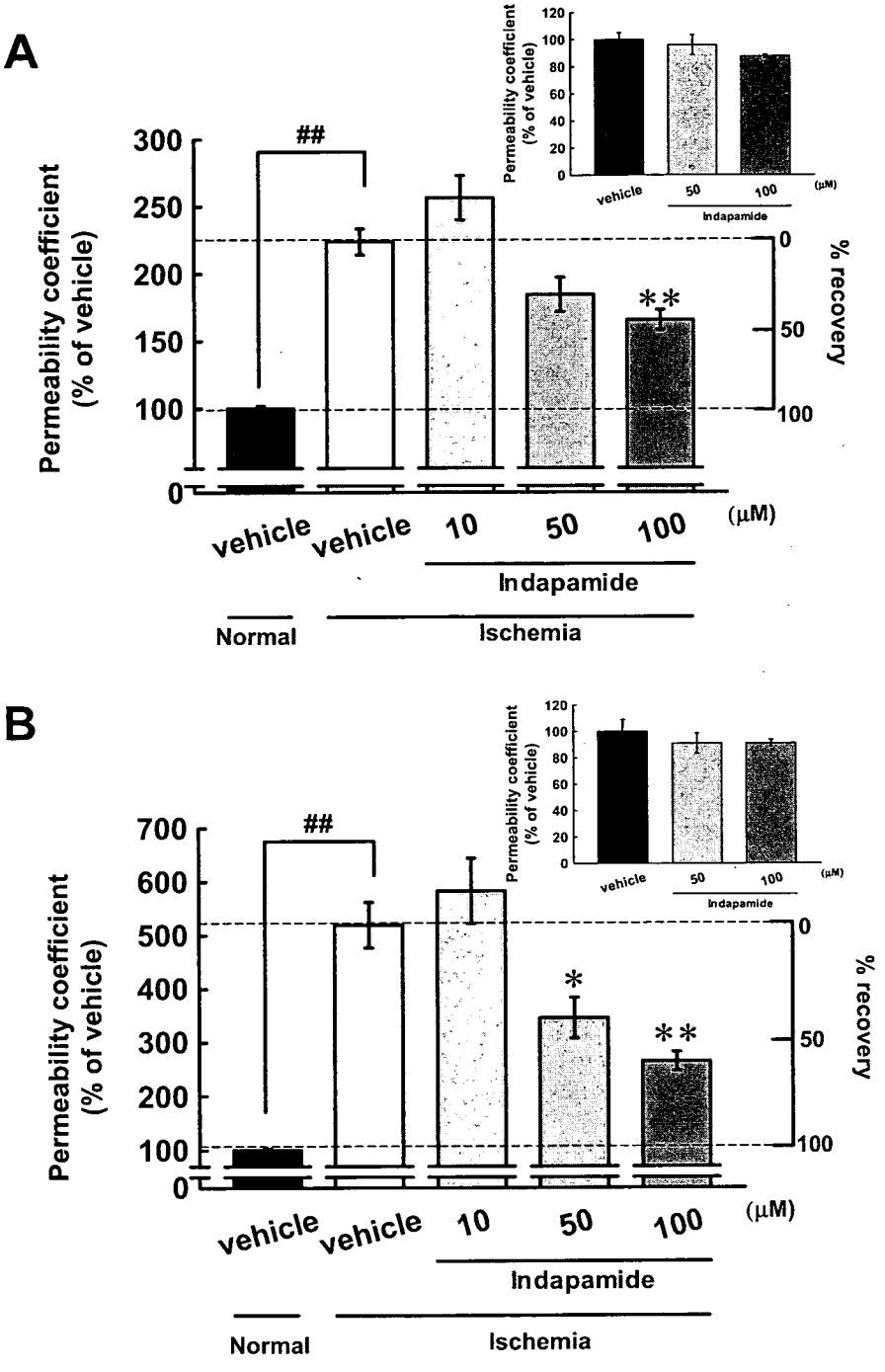

Fig. 2. Effects of indapamide on Na-F (A) and EBA (B) permeability in MBEC4 cell monolayer after a 7-h exposure to normal or ischemic conditions. The inset in each panel shows the effects of indapamide on permeability of the MBEC4 cell monolayer to Na-F and EBA after a 7-h exposure to normal conditions. The permeability coefficients of Na-F and EBA in the MBEC4 monolayer, after a 7-h exposure to normal conditions with vehicle treatment, were $3.109 \pm 0.012 \times 10^{-4}$ and $0.798 \pm 0.003 \times 10^{-4}$ cm/min, respectively. Results are expressed as % of vehicle under normal conditions with vehicle treatment. The % recovery is shown on the right-side of each panel and was calculated by the following equation: [% of vehicle under ischemia condition with indapamide treatment − % of vehicle under ischemia condition with vehicle treatment] / [% of vehicle under normal condition with vehicle treatment − % of vehicle under ischemic condition with vehicle treatment] × 100. Data are expressed as the mean ± S.E.M. (n = 8). $^{\#\#}P<0.01$, significant difference from vehicle under normal conditions. $^{*}P<0.05$, $^{**}P<0.01$, significant difference from vehicle under ischemic conditions.

ability coefficients of Na-F and EBA were significantly increased to 223.7 ± 9.8% and 518.9 ± 42.5% of the vehicle under normal conditions, respectively. The viability of MBEC4 cells grown on membranes after a 7-h exposure to ischemic conditions and following termination of the permeability test (2 h) were 72.8 ± 3.6% and 71.3 ± 1.0% of cells subjected to normal conditions, respectively; there was no difference in cell viability before and after the permeability test. Following a 7-h exposure to indapamide (50 − 100 μM) under ischemic conditions, hyperpermeability of MBEC4 cells to Na-F and EBA was concentration-dependently reduced by 31.9% − 47.4% and 41.4% − 60.6% of the vehicle, respectively. This effect was not accompanied by a change in cell viability (vehicle: 72.8 ± 3.6%, 100 mM: 75.9 ± 2.3%). Under normal conditions, these concentrations of indapamide had no effect on the permeability coefficients of Na-F and EBA in MBEC4 cells. These findings suggest that indapamide may efficiently inhibit ischemia-induced hyperpermeability rather than inhibit

ischemic cell death. MBEC4 cells that were grown on membranes exhibited a higher vulnerability to ischemic cytotoxicity and lower sensitivity to the cytoprotective action of indapamide than those grown on the smooth plastic surface of a well. Further experiments will be required to clarify these issues.

The in vitro ischemia/reperfusion conditions used in the present study significantly reduced the viability of MBEC4 cells, and this effect was ameliorated by indapamide. Ischemic conditions increased the permeability of MBEC4 cells to Na-F and EBA, but this hyperpermeability was reduced by indapamide.

Disruption of the BBB is a critical event during cerebral ischemia as it is followed by the passive diffusion of water, leading to vasogenic edema and secondary brain injury. Cerebral edema is a major and fatal complication of acute ischemic stroke. Free radical overproduction after brain ischemia and reperfusion contributes to brain edema and neuronal damage. Thus, an inhibition of free radical formation is likely to prevent the occurrence of brain edema and neuronal damage. Indapamide has an antioxidant effect and has the potential to scavenge oxygen free radicals and their derivatives. Boucher et al. reported that indapamide treatment has a protective effect on cardiac tissue during the early stages of postischemic reperfusion (6). The present findings suggest that indapamide may protect cerebral endothelial cells from ischemic damage due to antioxidation and/or free radical scavenging. This phenomenon may contribute, at least in part, to the mechanisms by which indapamide facilitated protection of perindopril against recurrent stroke in a recent clinical study (7).

Brain capillary endothelial cells form a metabolic and physical barrier that separates the periphery from the brain to maintain cerebral homeostasis. The lack of fenestrations and the presence of tight junctions differentiate brain microvessel endothelial cells from peripheral microvascular endothelium. While adherent junctions and other junctional proteins contribute to cell-to-cell contacts in the paracellular cleft, tight junctions are critical for restricting paracellular diffusion in the cerebral microvasculature. Increased cerebrovascular permeability is a principal factor in the development of cerebral edema after brain ischemia. Several studies have shown a relationship between cyclic AMP (cAMP) levels and permeability of endothelial cell monolayers. For example, elevation of intracellular cAMP concentrations induces high transendothelial electrical resistance and increases P-glycoprotein function in brain capillary endothelial cells (11, 12). In addition, when bovine aortic endothelial cells were cultured in hypoxic conditions, cellular cAMP levels decreased and this phenomenon was associated with an increase in cellular permeability (13). Furthermore, a decrease in cAMP levels was detectable after brain microvascular endothelial cells were exposed to hypoxic conditions for 3 h (14). Moreover, indapamide was shown to augment cAMP production induced by forskolin, an adenylyl cyclase activator, but did not alter basal cAMP levels in cardiomyocytes alone (15). Therefore, indapamide may protect cerebral microvascular endothelial cells from ischemic dysfunction by increasing intracellular cAMP levels. The effects of indapamide on the expression of tight junction-related proteins and on intracellular messengers are now being investigated in rat brain primary cultured endothelial cells.

We present here in vitro evidence to suggest a possible protective action of indapamide against ischemia/reperfusion-induced injury and dysfunction of the BBB.

Acknowledgments

Indapamide was kindly provided by Kyoto Pharmaceutical Industries Co., Ltd. This work was supported, in part, by Grants-in-Aid for Scientific Research ((B) 17390159) from JSPS, Japan and by a research fund from Fukuoka University (No. 003171PK; Sumitomo Pharma Co., Ltd.).

References

1 Pardridge WM. Blood-brain barrier biology and methodology. J Neurovirol. 1999;5:556–569.
2 Mark KS, Davis TP. Cerebral microvascular changes in permeability and tight junctions induced by hypoxia-reoxygenation. Am J Physiol Heart Circ Physiol. 2002;282:H1485–H1494.
3 Hayashi K, Nakao S, Nakaoke R, Nakagawa S, Kitagawa N, Niwa M. Effects of hypoxia on endothelial/pericytic co-culture model of the blood-brain barrier. Regul Pept. 2004;123:77–83.
4 Brown RC, Davis TP. Calcium modulation of adherens and tight junction function: a potential mechanism for blood-brain barrier disruption after stroke. Stroke. 2002;33:1706–1711.
5 O'Donnell ME, Tran L, Lam TI, Liu XB, Anderson SE. Bumetanide inhibition of the blood-brain barrier Na-K-Cl cotransporter reduces edema formation in the rat middle cerebral artery occlusion model of stroke. J Cereb Blood Flow Metab. 2004;24:1046–1056.
6 Boucher FR, Schatz CJ, Guez DM, de Leiris JG. Beneficial effect of indapamide in experimental myocardial ischemia. Am J Hypertens. 1992;5:22–25.
7 PROGRESS Collaborative Group. Randomised trial of a perindopril-based blood-pressure-lowering regimen among 6,105 individuals with previous stroke or transient ischaemic attack. Lancet. 2001;358:1033–1041.
8 Tatsuta T, Naito M, Oh-hara T, Sugawara I, Tsuruo T, Functional involvement of P-glycoprotein in blood-brain barrier.

J Biol Chem. 1992;267:20383–20391.
9 Dohgu S, Yamauchi A, Takata F, Naito M, Tsuruo T, Higuchi S, et al. Transforming growth factor-beta1 upregulates the tight junction and P-glycoprotein of brain microvascular endothelial cells. Cell Mol Neurobiol. 2004;24:491–497.
10 Dehouck MP, Jolliet-Riant P, Bree F, Fruchart JC, Cecchelli R, Tillement JP. Drug transfer across the blood-brain barrier: correlation between in vitro and in vivo models. J Neurochem. 1992;58:1790–1797.
11 Kis B, Deli MA, Kobayashi H, Abraham CS, Yanagita T, Kaiya H, et al. Adrenomedullin regulates blood-brain barrier functions in vitro. Neuroreport. 2001;12:4139–4142.
12 Deli MA, Abraham CS, Takahata H, Niwa M. Tissue plasminogen activator inhibits P-glycoprotein activity in brain endothelial cells. Eur J Pharmacol. 2001;411:R3–R5.
13 Ogawa S, Koga S, Kuwabara K, Brett J, Morrow B, Morris SA, et al. Hypoxia-induced increased permeability of endothelial monolayers occurs through lowering of cellular cAMP levels. Am J Physiol. 1992;262:C546–C554.
14 Fischer S, Renz D, Schaper W, Karliczek GF. Effects of barbiturates on hypoxic cultures of brain derived microvascular endothelial cells. Brain Res. 1996;707:47–53.
15 Rabkin SW. Indapamide alters the cyclic AMP signal transduction pathway in cardiomyocytes in culture. Eur J Pharmacol. 1994;266:117–123.

2-(2-[2-Dimethylaminothiazol-5-yl]Ethenyl)-6-(2-[Fluoro]Ethoxy)Benzoxazole: A Novel PET Agent for In Vivo Detection of Dense Amyloid Plaques in Alzheimer's Disease Patients

Yukitsuka Kudo[1], Nobuyuki Okamura[2], Shozo Furumoto[1], Manabu Tashiro[3], Katsutoshi Furukawa[4], Masahiro Maruyama[4], Masatoshi Itoh[3], Ren Iwata[5], Kazuhiko Yanai[2], and Hiroyuki Arai[4]

[1]Tohoku University Biomedical Engineering Research Organization (TUBERO), Sendai, Japan; [2]Department of Pharmacology, Tohoku University School of Medicine, Sendai, Japan; [3]Division of Cyclotron Nuclear Medicine, Cyclotron and Radioisotope Center, Tohoku University, Sendai, Japan; [4]Department of Geriatrics and Gerontology, Center for Asian Traditional Medicine, Tohoku University School of Medicine, Sendai, Japan; and [5]Division of Radiopharmaceutical Chemistry, Cyclotron and Radioisotope Center, Tohoku University, Sendai, Japan

Extensive deposition of dense amyloid fibrils is a characteristic neuropathologic hallmark in Alzheimer's disease (AD). Noninvasive detection of these molecules is potentially useful for early and precise detection of patients with AD. This study reports a novel compound, 2-(2-[2-dimethylaminothiazol-5-yl]ethenyl)-6-(2-[fluoro]ethoxy)benzoxazole (BF-227), for in vivo detection of dense amyloid deposits using PET. **Methods:** The binding affinity of BF-227 to amyloid-β (Aβ) fibrils was calculated. The binding property of BF-227 to amyloid plaques was evaluated by neuropathologic staining of AD brain sections. Brain uptake and in vivo binding of BF-227 to Aβ deposits were also evaluated using mice. For clinical evaluation of ^{11}C-BF-227 as a PET probe, 11 normal (healthy) subjects and 10 patients with AD participated in this study. Dynamic PET images were obtained for 60 min after administration of ^{11}C-BF-227. The regional standardized uptake value (SUV) and the ratio of regional to cerebellar SUV were calculated as an index of ^{11}C-BF-227 retention. The regional tracer distribution in AD patients was statistically compared with that of aged normal subjects on a voxel-by-voxel basis. **Results:** BF-227 displayed high binding affinity to synthetic Aβ1-42 fibrils (K_i [inhibition constant], 4.3 ± 1.5 nM). Neuropathologic staining has demonstrated preferential binding of this agent to dense amyloid deposits in AD brain. Moreover, a biodistribution study of this agent revealed excellent brain uptake and specific labeling of amyloid deposits in transgenic mice. The present clinical PET study using ^{11}C-BF-227 demonstrated the retention of this tracer in cerebral cortices of AD patients but not in those of normal subjects. All AD patients were clearly distinguishable from normal individuals using the temporal SUV ratio. Voxel-by-voxel analysis of PET images revealed that cortical BF-227 retention in AD patients is distributed primarily to the posterior association area of the brain and corresponded well with the preferred site for neuritic plaque depositions containing dense Aβ fibrils. **Conclusion:** These findings suggest that BF-227 is a promising PET probe for in vivo detection of dense amyloid deposits in AD patients.

J Nucl Med 2007; 48:553–561
DOI: 10.2967/jnumed.106.037556

Substantial neuropathologic evidence suggests that the deposition of senile plaques (SPs) and neurofibrillary tangles (NFTs) represents the characteristic neuropathologic hallmark in Alzheimer's disease (AD) (*1*). Progressive accumulation of SPs is considered fundamental to the initial development of dementia. Extensive deposition of SPs in the brain is present even in very mild AD and precedes the presentation of cognitive impairment (*2,3*). Several antiamyloid drugs are under development for the treatment and prevention of AD (*4*). For early detection and preventive intervention for AD, noninvasive imaging of neuropathologic lesions is a powerful strategy.

For this purpose, several imaging techniques have been developed that can noninvasively detect SPs in the brain using PET, SPECT, and MRI. Among these imaging modalities, PET is the most advanced and practical method for in vivo measurement of SP depositions. To achieve successful imaging using PET, various radiolabeled agents have been developed. Currently, 6OH-BTA-1 (PIB) is the most successful PET agent for in vivo amyloid imaging. This tracer sensitively detects amyloid fibrils in the brain and is proven to be useful for early diagnosis of AD (*5–7*).

However, amyloid-β (Aβ) deposition is also frequent in aging, even in cognitively intact individuals. Excessive identification of Aβ has a potential risk to misjudge the normal aging process with abnormal Aβ deposition. In the

Received Oct. 23, 2006; revision accepted Jan. 20, 2007.
For correspondence or reprints contact: Nobuyuki Okamura, MD, Department of Pharmacology, Tohoku University School of Medicine, 2-1, Seiryo-machi, Aoba-ku, Sendai 980-8575, Japan.
E-mail: oka@mail.tains.tohoku.ac.jp

normal aging process, noncompact or diffuse amyloid plaques containing less fibrillar Aβ are deposited primarily in the brain. Brains from patients with AD are characterized by an anatomically widespread process of amyloid deposition and neuritic plaque formation containing dense amyloid fibrils (*8*). A shift of brain Aβ from the soluble to the fibrillar form is closely associated with the onset of AD (*9*). Therefore, selective detection of dense amyloid fibrils would be advantageous to differentiate the normal aging process from AD with high specificity.

We have previously demonstrated a novel series of benzoxazole derivatives as promising candidates for an in vivo imaging probe of SPs (*10–12*). These derivatives showed comparatively high blood–brain barrier (BBB) permeability, high binding affinity for Aβ aggregates, and high specificity for fibrillar Aβ deposits, suggesting potential merit for the early detection of AD-related pathologies. Herein we introduce an optimized derivative, 2-(2-[2-dimethylaminothiazol-5-yl]ethenyl)-6-(2-[fluoro]ethoxy)benzoxazole (BF-227), as a PET probe for in vivo detection of dense amyloid deposits in humans.

MATERIALS AND METHODS

Preparation of Compounds

BF-227 (Fig. 1) and its *N*-desmethylated derivative (a precursor of ^{11}C-BF-227) were custom-synthesized by Tanabe R&D Service Co. ^{11}C-BF-227 was synthesized from the precursor by *N*-methylation in dimethyl sulfoxide (Fig. 1) using ^{11}C-methyl triflate (*13,14*). After quenching the reaction with 5% acetic acid in ethanol, ^{11}C-BF-227 was separated from the crude mixture by semipreparative reversed-phase high-performance liquid chromatography and then isolated from the collected fraction by solid-phase extraction. The purified ^{11}C-BF-227 was solubilized in isotonic saline containing 1% polysobate-80 and 5% ascorbic acid. The saline solution was filter-sterilized with a 0.22-μm Millipore filter for clinical use. The radiochemical yields were >50% based on ^{11}C-methyl triflate, and the specific radioactivities were 119–138 GBq/μmol at the end of synthesis. The radiochemical purities were >95%.

In Vitro Binding Assays

Binding affinities of the compounds for synthetic Aβ1-42 aggregates were examined as described previously (*10*). Briefly, solid-form Aβ1-42 (Peptide Institute) was dissolved in 10 mM potassium phosphate buffer (pH 7.4) and incubated at 37°C for 40 h. The binding assay was performed by mixing 100 μL of aggregated Aβ1-42 with the appropriate concentration of ^{125}I-labeled 2-(4-methylamino)styryl-5-iodo-benzoxazole (BF-180) and 8% ethanol. After incubation for 4 h at room temperature, the binding mixture was filtered and filters containing bound ^{125}I ligand were counted using a γ-counter. The dissociation constant (K_d) and maximum specific binding (B_{max}) of BF-180 were determined. For inhibition studies, binding studies were performed using synthetic Aβ1-42 aggregates. A mixture containing 50 μL of BF-227, 50 μL of 0.05 nM ^{125}I-BF-180, 100 μL of 100 nM Aβ1–42, and 800 μL of 8% ethanol was incubated at room temperature for 4 h. The mixture was then filtered through Whatman GF/B filters, and filters containing bound ^{125}I ligand were counted in a γ-counter. Values for the half-maximal inhibitory concentration (IC_{50}) were determined from displacement curves of 3 independent experiments using Prism software (GraphPad), and values for the inhibition constant (K_i) were determined using the Cheng–Prusoff equation.

Measurement of Octanol/Water Partition Coefficients

Phosphate-buffered saline (PBS) and 1-octanol (Wako) were saturated with 1-octanol and PBS, respectively, before use. BF-227 was dissolved in 1-octanol and shaken with equal amounts of PBS for 30 min at room temperature. After centrifugation at 2,000 rpm for 15 min, absorbency of the 1-octanol layer was measured at the peak wavelength of the absorbance spectrum of BF-227 using a Spectra Max 190 microplate reader (Molecular Devices). Octanol/water partition coefficients were determined by comparing absorbency with that before shaking with PBS. Each data point was performed in duplicate.

BBB Permeability of BF-227 in Normal Mice

Brain uptake of BF-227 was measured using ^{11}C-labeled compound. The ^{11}C-BF-227 (1.1–6.3 MBq) was administered into the tail vein of male C57B6 mice (n = 23; mean weight, 28–32 g). Mice were then sacrificed by decapitation at 2, 10, 30, and 60 min after injection. The whole brain was removed and weighed, and radioactivity was counted using an automatic γ-counter. The percentage injected dose per gram of tissue (%ID/g) was calculated by normalizing tissue counts to tissue weight. Each %ID/g value is expressed as a mean ± SD of 3 or 4 separate experiments.

Neuropathologic Staining

Postmortem brain tissues from a 69-y-old man with autopsy-confirmed AD and an 81-y-old man with autopsy-confirmed physiologic aging were obtained from Fukushimura Hospital (Toyohashi, Japan). Experiments were performed under the regulations of the ethics committee of BF Research Institute. Serial sections (6-μm thick) from paraffin-embedded blocks of temporal cortex, striatum, and cerebellum were prepared in xylene and ethanol. Before

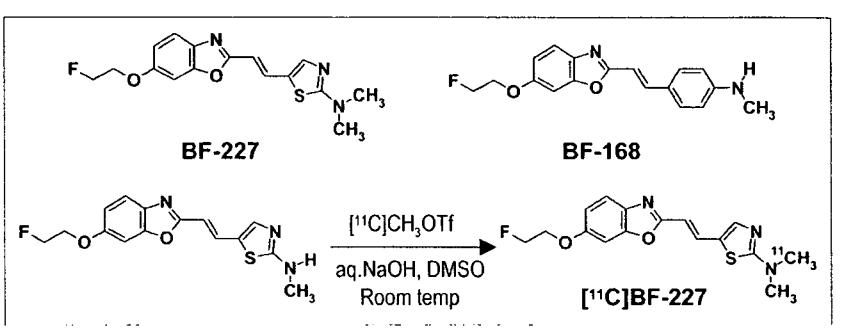

FIGURE 1. Chemical structures of BF-227 and BF-168 and radiosynthesis of BF-227.

the staining of compounds, quenching of autofluorescence was performed as described previously. Quenched tissue sections were immersed in 100 μM of BF-227 or 0.125% thioflavin-S solution containing 50% ethanol for 10 min. Sections stained with each compound were then dipped briefly into water and rinsed in PBS for 60 min before coverslipping with Fluor Save Reagent (Calbiochem); sections were examined using an Eclipse E800 microscope (Nikon) equipped with a V-2A filter set (excitation, 380–420 nm; dichroic mirror, 430 nm; long-pass filter, 450 nm). Sections stained with thioflavin-S were dipped briefly in tap water and in 50% ethanol and then washed in PBS for 60 min before coverslipping; this was followed by fluorescent microscopy using a BV-2A filter set (excitation, 400–440 nm; dichroic mirror, 455 nm; long-pass filter, 470 nm). In addition, adjacent sections were immunostained using monoclonal antibody (mAb) against Aβ (6F/3D; Dako A/S). After pretreatment with 90% formic acid for 5 min, sections were immersed in blocking solution for 30 min and then incubated for 60 min at 37°C with 6F/3D at a dilution of 1:50. After incubation, sections were processed by the avidin–biotin method using a Pathostain ABC-POD(M) Kit (Wako) and diaminobenzidine tetrahydrochloride.

Labeling of Aβ Deposits in Transgenic Mouse Brain

Ex vivo plaque labeling with BF-227 was evaluated using PS1/APPsw double transgenic mice (n = 2) and a wild-type mouse (n = 1) (male, 32-wk old) (*15*). A BF-227 solution containing 10% polyethylenglycol 400 and 0.1 mol/L HCl was administered into the tail vein at a dose of 4 mg/kg. Mice were anesthetized using sodium pentobarbital 2 h after injection of BF-227; they were then perfused transcardially with ice-cold saline, which was followed by 4% paraformaldehyde in 0.1 M PBS, and the brains were removed. After cryoprotection in 30% sucrose/0.1 M PBS, 6-μm frozen sections were cut using an OTF cryostat and imaged with no additional staining for fluorescent microscopy using a V-2A filter set. The same sections were immunostained using mAb against Aβ (6F/3D) as described earlier.

Subjects and Patients in Clinical PET Study

Eleven normal (healthy) control subjects, including 3 young normal subjects and 8 aged-matched normal subjects, and 10 probable AD patients underwent PET measurement of ^{11}C-BF-227 distribution in the brain (Table 1). AD patients were recruited through the Tohoku University Hospital Dementia Patients Registry. The diagnosis of AD was made according to the National Institute of Neurological and Communicative Diseases and Stroke/Alzheimer's Disease and Related Disorders Association (NINCDS–ADRDA) criteria. The normal control group was recruited from volunteers, who were taking no centrally acting medication, had no cognitive impairment, and had no cerebrovascular lesion on MR images. No significant difference in age was apparent between the AD group and the aged normal control group. AD patients had significantly lower mean mini-mental status examination (MMSE) scores than normal control subjects. This study was approved by the ethics committee on clinical investigations of Tohoku University School of Medicine and was performed in accordance with the Declaration of Helsinki. After complete description of the study to the patients and subjects, written informed consent was obtained.

Image Acquisition Protocols

The protocol of the PET study was approved by the Committee on Clinical Investigation at The Tohoku University School of Medicine and the Advisory Committee on Radioactive Substances at Tohoku University. The ^{11}C-BF-227 PET study was performed using a SET-2400W PET scanner (Shimadzu). After intravenous injection of 211–366 MBq of ^{11}C-BF-227, dynamic PET images were obtained for 60 min (23 sequential scans: 5 scans × 30 s, 5 scans × 60 s, 5 scans × 150 s, and 8 scans × 300 s) with each subject's eyes closed. The T1-weighted MR images were obtained using a SIGNA 1.5-T machine (GE Healthcare).

TABLE 1
Subject Demographics

Group	Subject	Sex	Age (y)	MMSE score
Young normal (n = 3)	YN 1	M	36	30
	YN 2	M	37	30
	YN 3	M	36	30
	Mean ± SD		36.3 ± 0.6	30.0 ± 0.0
Aged normal (n = 8)	AN 1	M	69	30
	AN 2	F	70	29
	AN 3	F	64	30
	AN 4	F	65	30
	AN 5	M	67	30
	AN 6	M	69	30
	AN 7	M	71	30
	AN 8	M	59	30
	Mean ± SD		66.8 ± 4.0	29.9 ± 0.4
All normal (n = 11)	Mean ± SD		58.5 ± 14.6	29.9 ± 0.3
AD (n = 10)	AD 1	F	65	24
	AD 2	M	75	19
	AD 3	F	72	21
	AD 4	F	82	18
	AD 5	F	62	20
	AD 6	F	68	21
	AD 7	M	70	23
	AD 8	F	85	23
	AD 9	M	78	14
	AD 10	F	75	26
	Mean ± SD		73.2 ± 7.3*	20.9 ± 3.4*†

*P < 0.05 vs. young normal group.
†P < 0.05 vs. aged normal group.
MMSE = mini-mental state examination.

Image Analysis

First, standardized uptake value (SUV) images of ^{11}C-BF-227 were obtained by normalizing tissue radioactivity concentration by injected dose and body weight. Subsequently, individual MR images were anatomically coregistered into individual PET images using Statistical Parametric Mapping software (SPM2; Wellcome Department, U.K.) (*16*). Regions of interest (ROIs) were placed on individual axial MR images in the cerebellar hemisphere, striatum, thalamus, frontal cortex (Brodmann's areas [BA] 8, 9, 10, 44, 45, 46, and 47), lateral temporal cortex (BA 21, 22, 37, and 38), parietal cortex (BA 39 and 40), temporooccipital cortex (BA 18 and 19), occipital cortex (BA 17), medial temporal cortex (BA 27, 28, 34, and 35), pons, and subcortical white matter, as described previously (*17*). The ROI information was then copied onto dynamic PET SUV images, and regional SUVs were sampled using Dr.View/LINUX software (Asahi-Kasei Joho System).

The interrater reliability for the ROI measurement was tested between 2 raters in 14 subjects and patients. The intraclass correlation coefficient was 0.95 in the frontal cortex and cerebellum, 0.97 in the lateral temporal and parietal cortices, and 0.98 in the medial temporal cortex. The correlation coefficient between these 2 measurements was 0.96 in the frontal cortex, 0.97 in the lateral temporal cortex, and 0.99 in the parietal cortex, medial temporal cortex, and cerebellum. SUVs between 40 and 60 min were averaged to calculate the SUVs for group comparison.

Statistical Analysis

For statistical comparison in the 3 groups, we applied the Kruskal–Wallis test, which was followed by Dunn's multiple comparison test. The difference in time–activity curves in ^{11}C-BF-227 PET was also evaluated by repeated measures ANOVA, which was followed by the Bonferroni–Dunn post hoc test. For statistical comparisons of PET measurements in aged normal and AD groups, we used the Mann–Whitney *U* test. Effect-size coefficients (Cohen's *d*) were also calculated for the evaluation of group differences in PET measurements. Statistical significance for each analysis was defined as $P < 0.05$. Statistical comparison between images from normal control subjects and AD patients was performed on a voxel-by-voxel basis using SPM2 software (*16*). SUV summation images 30–60 min after injection were stereotactically normalized using individual MR images into a standard space of Talairach and Tournoux. The normalized images were smoothed using a 16 × 16 × 16 mm gaussian filter. The count of each voxel was normalized to the cerebellar ROI value, because cerebellum is reported to be a region free of fibrillar amyloid plaques in AD brain. Images of patients with AD ($n = 10$) were compared with those of aged normal control subjects ($n = 8$) for between-group analysis ($P < 0.001$, uncorrected; extent threshold, $k = 200$). For the group analysis, a 2-sample *t* test was used to detect differences between the AD and normal control groups.

RESULTS

In Vitro Binding Study for Aβ Fibrils

In vitro binding assay indicated that BF-227 shows high binding affinity for Aβ1-42 fibrils. K_i for Aβ1-42 fibrils in competitive binding assay using ^{125}I-BF-180 was 4.3 ± 1.5 nM in BF-227, comparable to levels previously reported for compound BF-168.

Neuropathologic Staining in AD Brain Sections

Neuropathologic examination using BF-227 indicated that amyloid plaques were selectively stained with BF-227 in AD brain sections (Fig. 2A). Especially, cored plaques were brightly stained with BF-227, indicating that this compound preferentially binds to mature amyloid plaque. This staining pattern correlated well with Aβ immunostaining in adjacent sections (Fig. 2B, arrows). BF-227 staining was further compared with staining using thioflavin-S. In contrast to clear staining of SPs and NFTs with thioflavin-S (Fig. 2C), BF-227 primarily stained SPs, with faint staining of NFTs (Fig. 2B, arrowheads). No apparent staining was also observed in the temporal brain section of the aged normal case (Fig. 2D).

BBB Permeability and Clearance from Normal Brain

Next, we investigated whether BF-227 entered the brain in amounts sufficient for use as a PET agent. The log *P* value of BF-227 was 1.75, close to that of BF-168 (log $P = 1.79$). Intravenous administration of BF-227 into normal mice indicated that this compound readily penetrated the BBB. Brain uptakes at 2, 10, 30, and 60 min after intravenous injection of ^{11}C-BF-227 were 7.9 ± 1.3, 3.7 ± 0.37, 1.4 ± 0.36, and 0.64 ± 0.15 %ID/g, respectively. ^{11}C-BF-227 displayed double the initial uptake and faster washout

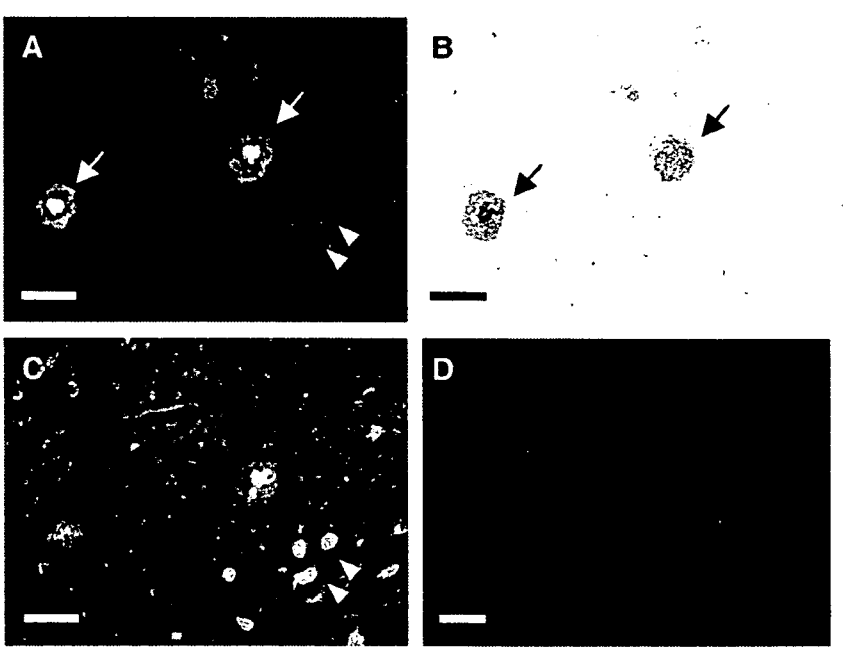

FIGURE 2. Neuropathologic staining of human brain sections by BF-227. Amyloid plaques are clearly stained with BF-227 in AD temporal brain sections (A). BF-227 staining correlates well with Aβ immunostaining in adjacent sections (B, arrows). BF-227 faintly stains NFTs, in contrast to clear staining with thioflavin-S (C, arrowheads). In aged normal temporal cortex (D), no staining by BF-227 is observed. Bar in A–C = 50 μm; bar in D = 200 μm.

in normal brain tissue compared with those of ^{18}F-BF-168 (3.9 %ID/g at 2 min after injection; 1.3 %ID/g at 60 min after injection).

Intravenous Administration of BF-227 in Transgenic Mice

In vivo binding of nonlabeled BF-227 to Aβ deposits was examined using PS1/APPsw double transgenic mice. After intravenous injection of 4 mg/kg BF-227, ex vivo observation of transgenic mouse brain slices showed numerous fluorescent spots in the neocortex and hippocampus (Figs. 3A and 3B). In contrast, no fluorescent spots were detected in the wild-type mouse brain (Fig. 3C). Brain sections of transgenic mice were subsequently immunostained using Aβ-specific antibody, and the distribution of plaques labeled with BF-227 corresponded well with Aβ immunostaining (Fig. 3D, arrowheads).

Time–Activity Data of ^{11}C-BF-227 in Clinical PET Study

No toxic event was observed in the current clinical trial of ^{11}C-BF-227. The SUV time–activity curves from ^{11}C-BF-227 PET in AD patients and all normal subjects are shown in Figure 4. Both groups showed rapid entry of ^{11}C-BF-227 into gray matter areas. In AD patients, the frontal, temporal, and parietal cortices, areas known to contain high concentrations of fibrillar amyloid plaques in AD, retained ^{11}C-BF-227 to a greater extent during the later time points compared with normal subjects (Figs. 4A–4C). When the 2 groups were compared, a significant difference in time–activity curves was observed in the frontal (Fig. 4A), lateral temporal (Fig. 4B), parietal (Fig. 4C), and visual association cortices (data not shown). In contrast, time–activity curves in the cerebellum (Fig. 4D), an area lacking fibrillar amyloid plaques, were nearly identical in normal subjects and AD patients. The subcortical white matter region showed relatively lower entry and slower clearance than gray matter areas but no significant difference in time–activity curves between the 2 groups (data not shown). In the comparison of time–activity curves in the cortical areas and cerebellum, AD patients showed a significant difference in time–activity curves over 10 min after administration of ^{11}C-BF-227, but normal subjects showed no significant differences.

SUV Images in AD Patients and Normal Control Subjects

SUV images summed over 20–40 min after injection of an aged normal subject (70-y-old woman) and an AD patient (68-y-old woman; MMSE score = 21) are shown in Figure 5. Cortical retention of ^{11}C-BF-227, especially in the basal portion of the frontal, temporal, and parietal region, was evident in the AD patient, in contrast with the images of the aged normal subject. This pattern of distribution is consistent with the findings of neuritic plaque distribution in postmortem AD brains (*18*). Higher retention of ^{11}C-BF-227 was also observed in the brainstem and thalamus; however, similar retention in these areas was detected in the aged normal subject. ^{11}C-BF-227 uptake in the cerebellum was relatively sparse in both the aged normal subject and the AD patient.

Comparisons of Regional SUVs and SUV Ratios

In the quantitative comparison of regional SUVs between 40 and 60 min after administration, cortical regions showed the tendency to be increased in AD patients; however, the difference was not significant because of the large individual difference in SUVs. SUVs in the thalamus, pons, and white matter were similar in the 3 groups. Because there were no plaques in the cerebellum, there was no BF-227 binding and no significant difference in the SUV between AD and normal groups, indicating that the cerebellum is adequate as a reference region. Therefore, the ratio of regional SUV to cerebellar SUV (SUV ratio) was calculated as an index of ^{11}C-BF-227 retention. This analysis successfully reduced the intersubject variability, as reflected in low SD values (Table 2). The mean SUV ratio for the frontal, lateral temporal, parietal, temporooccipital, occipital, anterior and posterior cingulate cortices, and striatum was significantly greater in AD patients than that in aged normal subjects (Table 2; Fig. 6). Notably, the SUV ratio in the lateral temporal cortex showed no overlap between AD patients and normal control subjects (Fig. 6). The SUV ratio in the medial temporal cortex, thalamus,

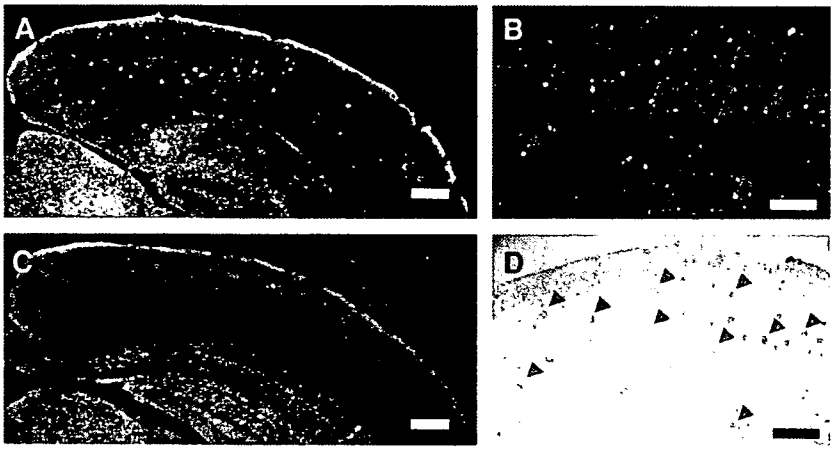

FIGURE 3. In vivo binding of BF-227 to amyloid plaques in PS1/APP transgenic mouse. In brain sections from PS1/APP transgenic mouse after intravenous injection of 4 mg/kg BF-227, numerous fluorescent spots were observed in neocortex and hippocampus of brain (A and B). In contrast, no fluorescent spots were observed in brain of wild-type mouse (C). Distribution of plaques labeled with BF-227 corresponded well with Aβ immunostaining in same section (B and D, arrowheads).

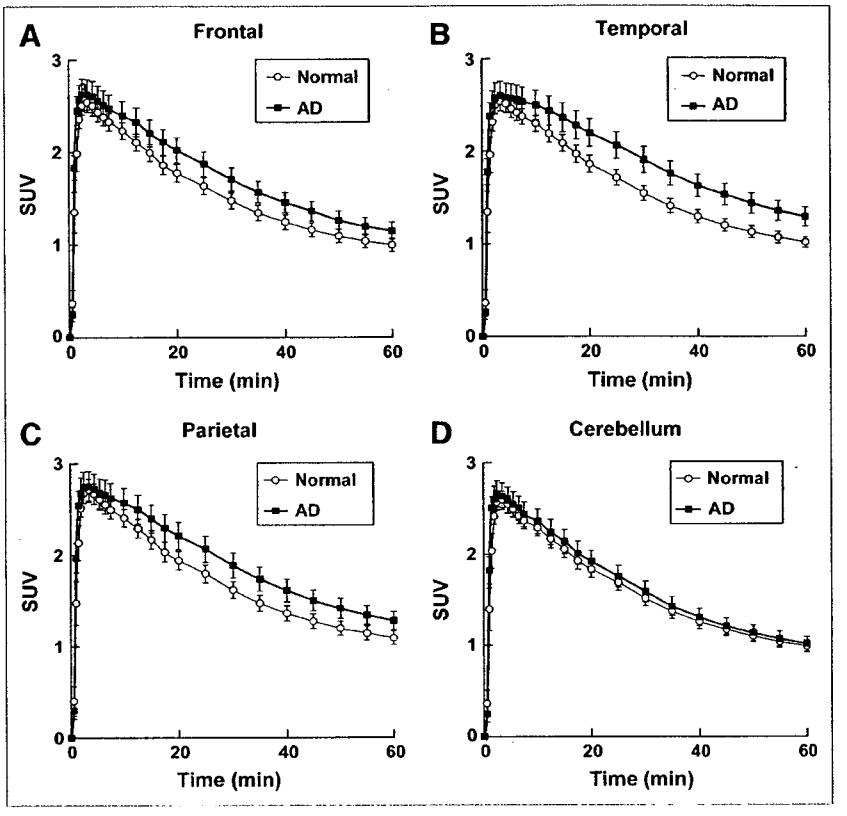

FIGURE 4. Time–activity data for ^{11}C-BF-227 PET in humans. SUV time–activity curves of ^{11}C-BF-227 in frontal cortex (A), temporal cortex (B), parietal cortex (C), and cerebellum (D) are shown. Each point represents mean ± SEM of data from 7 AD patients and 7 normal control subjects.

pons, and white matter was nearly identical in AD patients and normal subjects. The effect size between AD patients and aged normal subjects was highest in the lateral temporal cortex, which was followed by the parietal, anterior cingulate, and frontal cortices, and was lowest in the medial temporal, thalamus, and pons (Table 2). No significant difference was observed in any brain regions between young normal and aged normal subjects, although aged individuals tended to exhibit a higher SUV ratio in the frontal cortex than young individuals (data not shown).

Voxel-by-Voxel Analysis of ^{11}C-BF-227 PET Images

In comparison with aged normal subjects, AD patients showed significantly higher uptake of ^{11}C-BF-227 in the bilateral temporoparietal region ([50, −56, 6], Z = 5.41, k = 22,823), including the posterior cingulate cortex and the left middle frontal gyrus ([−26, 24, 40], Z = 3.79, k = 1,401) in SPM analysis (Fig. 7). These areas corresponded well with the region containing a high density of neuritic plaques. In contrast, no significant region was detected showing lower uptake of ^{11}C-BF-227 in the AD group than that in the normal group.

DISCUSSION

BF-227 was designed to improve BBB penetration and clearance from normal brain tissue, without deteriorating the high binding affinity of benzoxazole derivatives to Aβ. Several lipophilic compounds have been reported as potential amyloid imaging probes. 2-(1-{6-[(2-Fluoroethyl)(methyl)amino]-2-naphthyl}ethylidene)malononitrile (FDDNP) was introduced as the first BBB-permeable compound for in

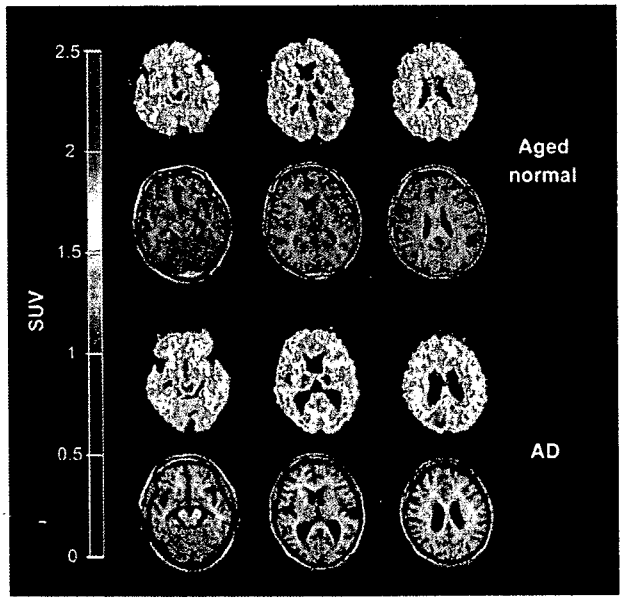

FIGURE 5. Mean SUV images between 20 and 40 min after injection of ^{11}C-BF-227 in aged normal subject (top, 70-y-old woman) and AD patient (bottom, 68-y-old woman). Coregistered MR images are shown below PET images.